Electronic Supplementary Material (ESI) for Chemical Science.
This journal is © The Royal Society of Chemistry 2021

Electronic Supplementary Information

Acid-Catalysed Liquid-to-Solid Transitioning of Arylazoisoxazole Photoswitches

Luuk Kortekaas,[a,]* Julian Simke,[a] Niklas B. Arndt,[a] Marcus Böckmann,[b] Nikos L. Doltsinis[b] and Bart Jan Ravoo[a,c,]**

[a]Center for Soft Nanoscience and Organisch-Chemisches Institut, Westfälische Wilhelms-Universität Münster, Busso-Peus-Straße 10, 48149 Münster, Germany

[b]Institute for Solid State Theory and Center for Multiscale Theory & Computation, Westfälische Wilhelms-Universität Münster, Wilhelm-Klemm-Str. 10, 48149 Münster, Germany

[c]Lead Contact

*Correspondence: kortekaas@uni-muenster.de

**Correspondence: b.j.ravoo@uni-muenster.de

Table of Contents

SUPPORTING DATA

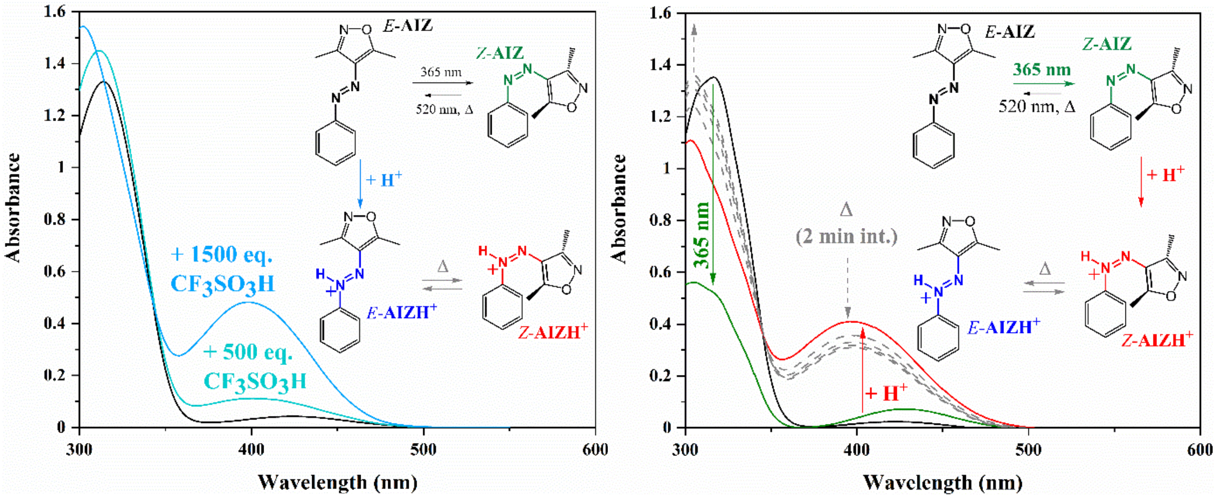

Figure S1. Protonation of AIZ 1 by UV/vis spectroscopy, Related to "Azonium formation in azoheterocycles". (Left) UV/vis absorption spectrum of AIZ **1** (70 µM in acetonitrile) before (black) and after addition of 500 (teal) and a further 1000 (navy) equivalents of CF_3SO_3H. The absorption of *E*-AIZH$^+$ seems to be blue-shifted, whereas the band at 400 nm presumably belongs to *Z*-AIZH$^+$ stemming from the thermal equilibrium with *E*-AIZH$^+$. (Right) UV/vis absorption spectrum of AIZ **1** (70 µM in acetonitrile) before (black) and after irradiation at 365 nm to form predominantly the *Z*-form (green). Subsequent addition of 1500 eq. CF_3SO_3H leads to formation of *Z*-AIZH$^+$ as observed at 400 nm (red line), which re-equilibrates to form *E*-AIZH$^+$ in the new thermal equilibrium between protonated forms (grey dashed lines, 2 min intervals).

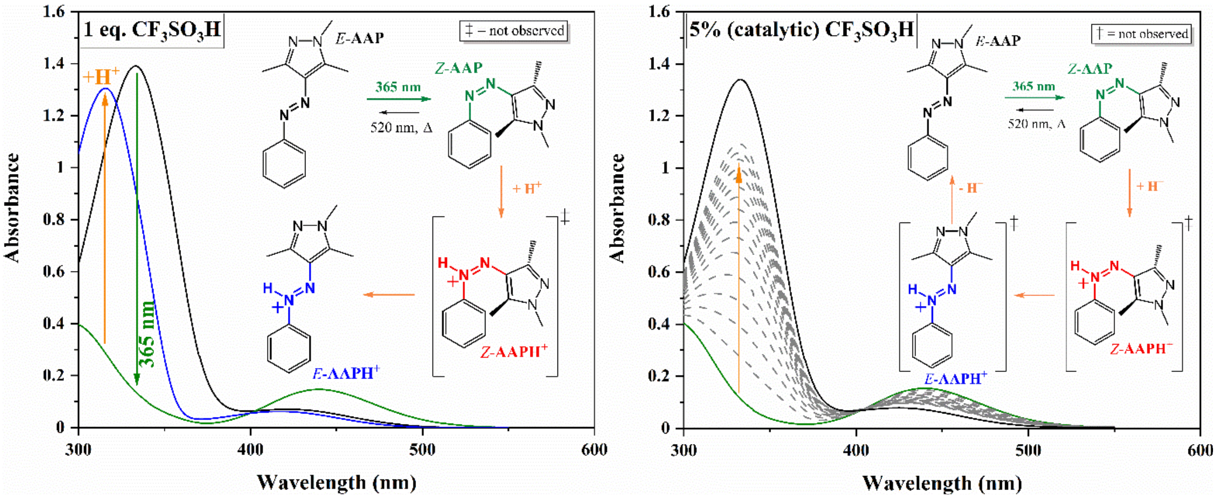

Figure S2. Protonation of AAP 4 by UV/vis spectroscopy, Related to "Azonium formation in azoheterocycles". (Left) UV/vis absorption spectrum of AAP **4** (70 µM in acetonitrile) before (black) and after irradiation at 365 nm (green). Subsequent addition of 10 equivalents of CF_3SO_3H (blue) leads to a blue shift which was also observed upon direct addition of 1000 eq. of CF_3SO_3H to the *E*-AAP **4**. (Right) UV/vis absorption spectrum of AAP **4** (70 µM in acetonitrile) before (black) and after irradiation at 365 nm (green), with addition of 0.05 eq. CF_3SO_3H leading to slow catalytic reversion to the *E*-AAP (grey dashed lines, 1 min intervals). *Z*- to *E*-reversion with catalytic amounts of strong acids is also observed for AIZ (see "**Thermally stable Z- and E-protonation with strong acids**").

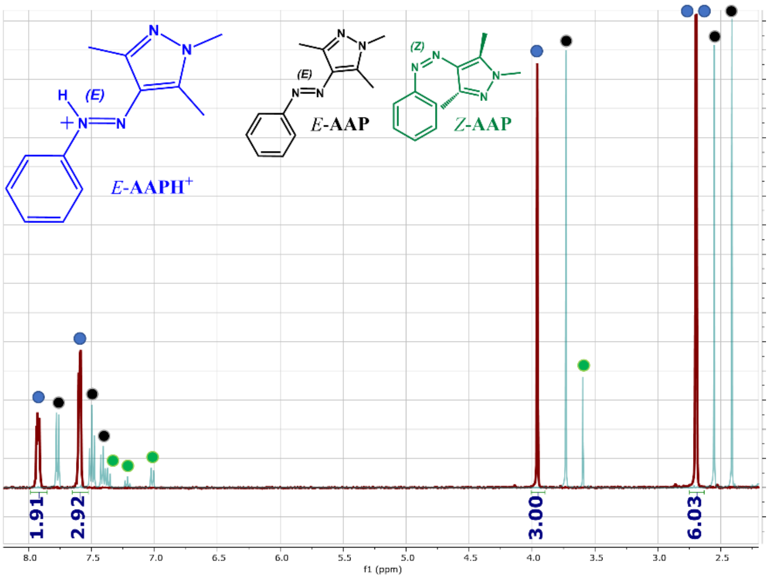

Figure S3. Protonation of AAP 4 by ^{1}H NMR spectroscopy, Related to "Azonium formation in azoheterocycles". ^{1}H NMR spectroscopy of AAP **4** (red lines, 3.3 mM in CD_3CN) after direct addition of 15 eq. of CF_3SO_3H to form *E*-AAPH⁺ (the background spectrum shows the chemical shifts of the unprotonated forms in blue). (400 MHz, CD_3CN) δ = 7.93 (m, 2H), 7.59 (m, 3H), 3.96 (s, 3H), 2.70 (s, 3H), 2.69 (s, 3H) ppm. The downfield shift upon protonation is also observed for AIZ **3** (see Table S1).

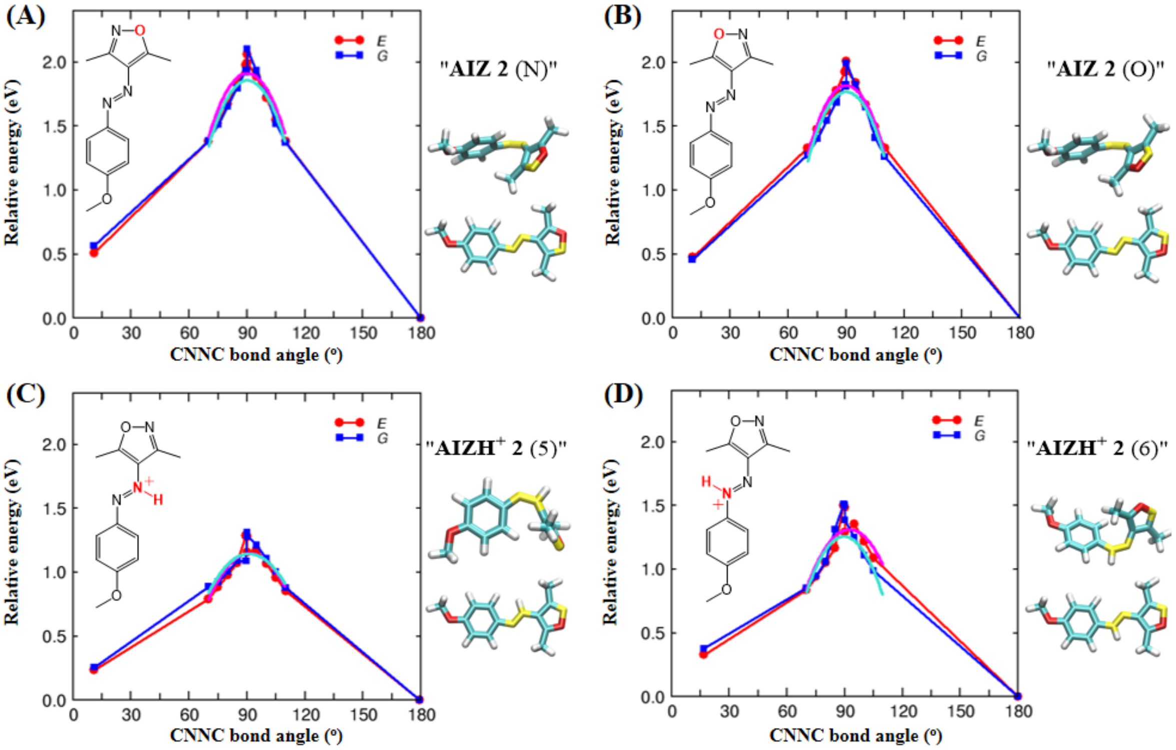

Figure S4. Calculated Gibbs free energies of AIZ 2, Related to "Azonium formation in azoheterocycles". Relative potential and free energies of (a, b) AIZ **2** (two orientations of the 5-ring) and (c, d) AIZH⁺ **2** (two positions of H⁺, at the 5-ring and at the 6-ring) calculated at the PCM/GD3BJ/B3LYP/6-31G* level of DFT theory; magenta and cyan lines indicate harmonic fit to obtain transition state energies.

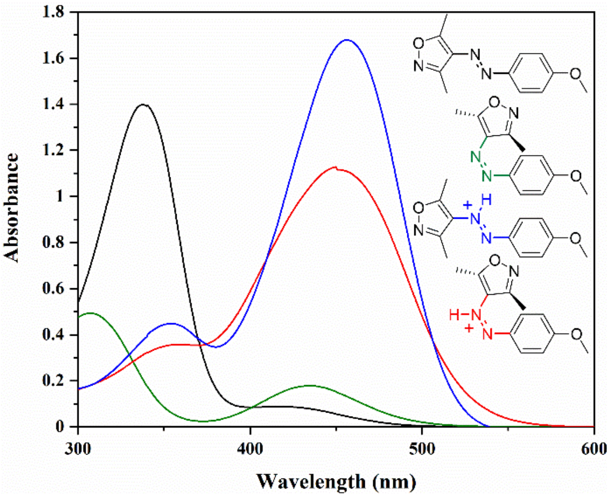

Figure S5. UV/vis absorbance of the various AIZ 2 species, Related to “Azonium formation in azoheterocycles”. UV/vis absorption of AIZ **2** (70 µM in acetonitrile) at thermal equilibrium in the E-form (black, 99% *E*-form) and at the PSS_{365nm} in the thermally stable Z-form (green, 97% *Z*-form). Addition of 1500 and 1000 eq. of CF_3SO_3H under these conditions yielded the absorption of the singly protonated *E*-AIZH⁺ (blue) and *Z*-AIZH⁺ (red) forms, respectively.

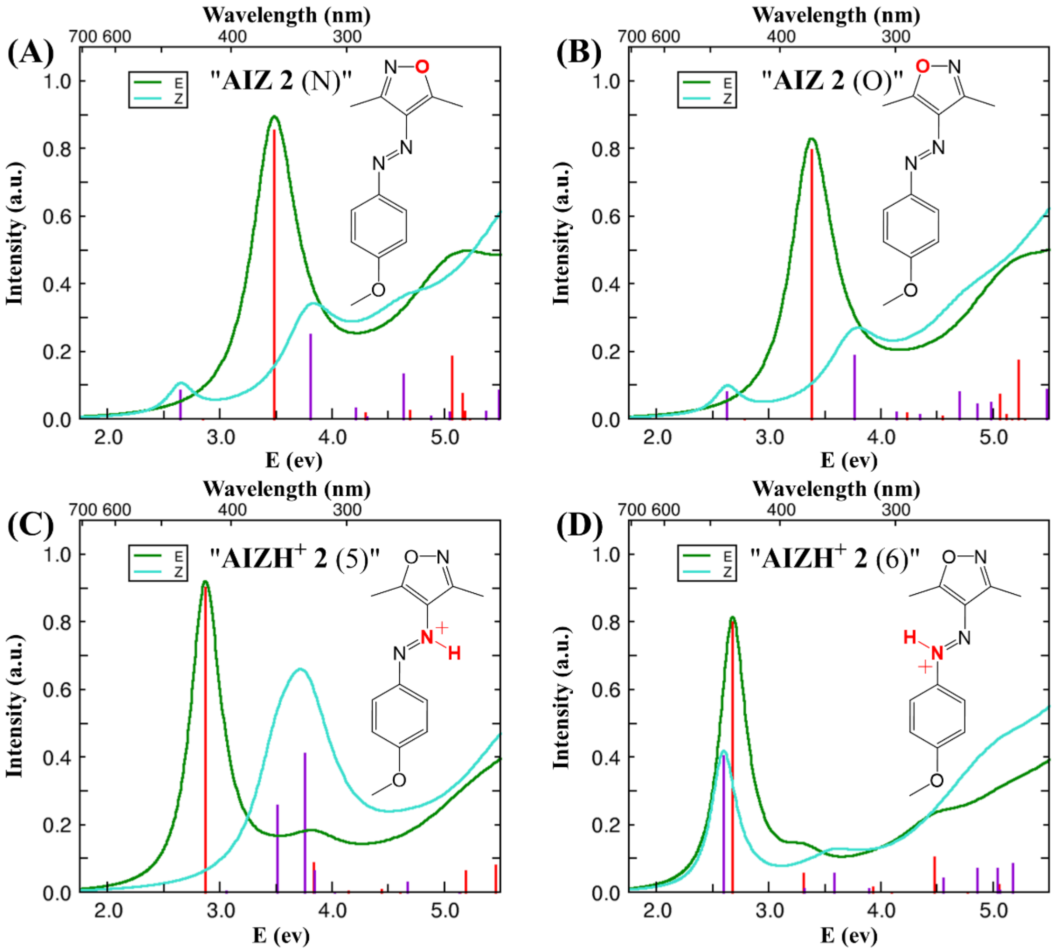

Figure S6. Calculated UV/vis spectra of AIZ 2, Related to “Azonium formation in azoheterocycles”. Line spectra obtained from TDDFT PCM/B3LYP/6-31G* calculations together with envelopes obtained from Lorentzian line broadening with fwhm = 50 nm for (a, b) AIZ **2** (two orientations of the 5-ring) and (c, d) AIZH⁺ **2** (two positions of H⁺).

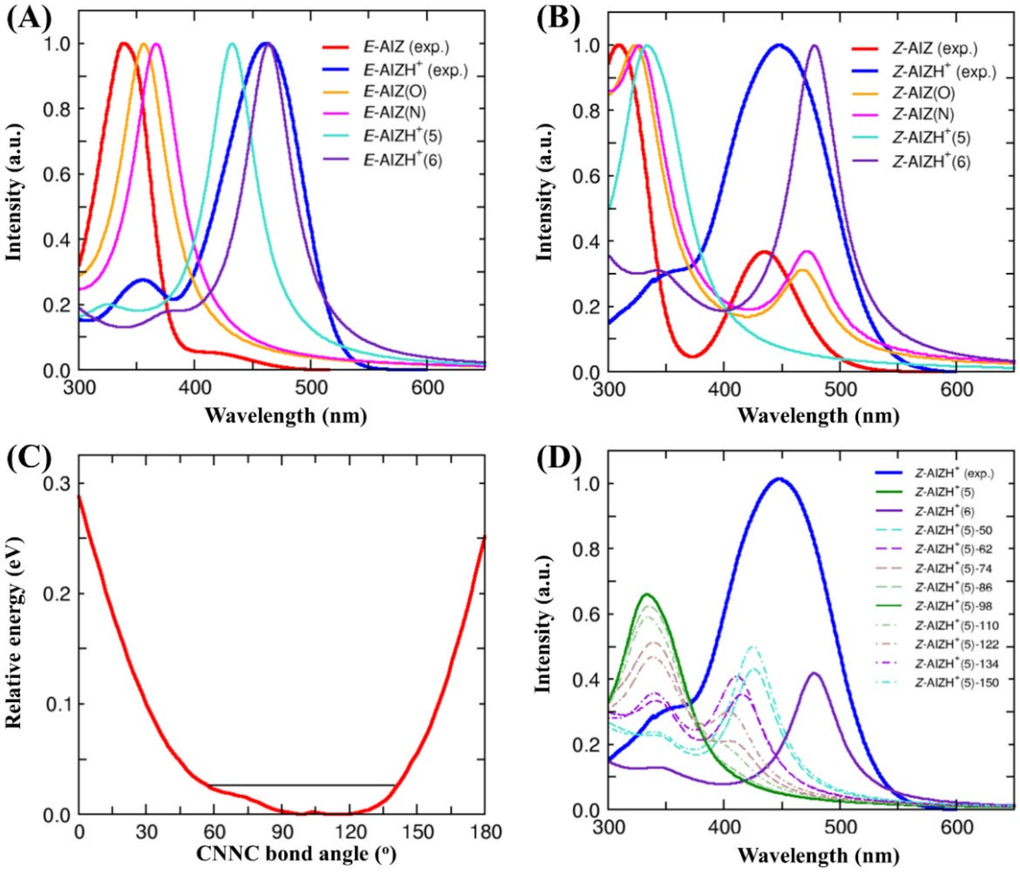

Figure S7. Comparison between experimental and calculated spectra of AIZ 2, Related to "Azonium formation in azoheterocycles". For the (A) *E*-conformer, the broad band of the protonated species can be explained by contributions from both protonation sites (see Figure S6 for corresponding structures); for the (B) *Z*-conformer, the calculated spectra for the optimized structures display insufficient contribution to the experimental band, but rotation of the 5-membered ring, which is (C) energetically within kB T (black line) at room temperature, yields (D) a significant rising signal (numbers in the legend indicate the rotation in degrees).

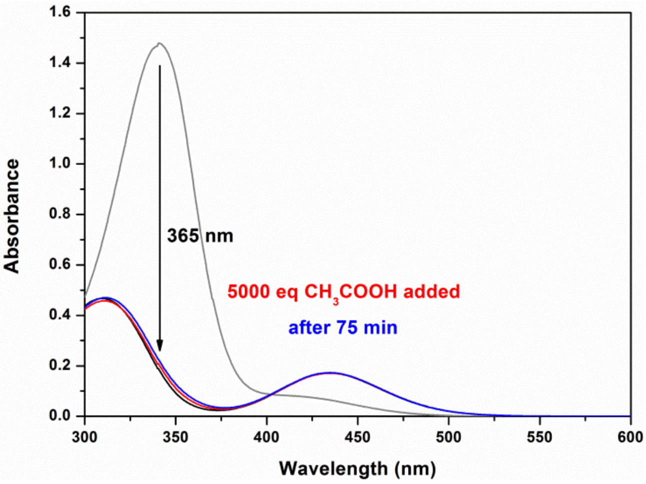

Figure S8. UV/vis spectroscopy of AIZ 3 with CH_3COOH, Related to "Accelerated *Z*- to *E*-reversion with weak acids". UV/vis absorption spectrum of AIZ **3** (70 µM in acetonitrile) before (grey) and after (black) *E*- to *Z*-isomerization at 365 nm, followed by addition of 5000 equivalents of acetic acid (red) and 75 min of waiting (blue). The lack of response versus CF_3COOH suggests that the pK_a of *Z*-AIZH$^+$ is intermediate to CH_3COOH and CF_3COOH.

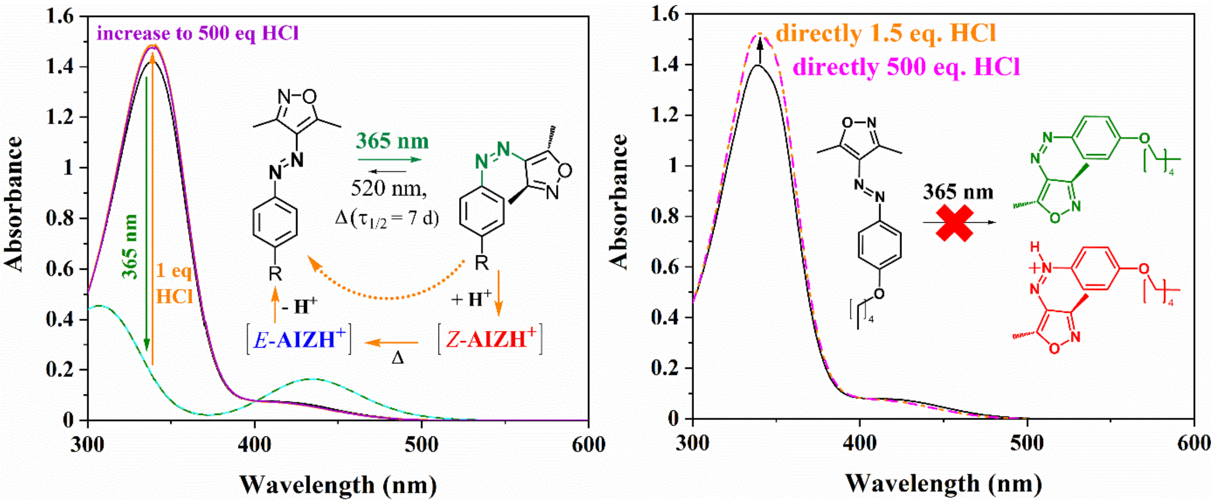

Figure S9. UV/vis spectroscopy of AIZs 2 and 3 with HCl, Related to "Accelerated *Z*- to *E*-reversion with weak acids". (Left) UV/vis absorption spectrum of AIZ **2** (70 µM in acetonitrile) before (solid black line) and after (dashed line) reaching the PSS_{365nm}. Adding 1 eq. of HCl leads to rapid reisomerization to the unprotonated *E*-form (yellow line), with subsequent increase to 500 eq. of HCl leading to no further changes (purple line, overlapping yellow). (Right) UV/vis absorption spectrum of AIZ **3** (70 µM in acetonitrile) before (solid black line) and after (yellow dashed line) adding 1.5 equivalents of HCl directly. Alike with AIZ **2**, the 1.5 equivalents cause thermal instability in what little *Z*-form is present, no further changes in absorption are observed upon incremental addition of HCl up to 500 equivalents (magenta dashed line).

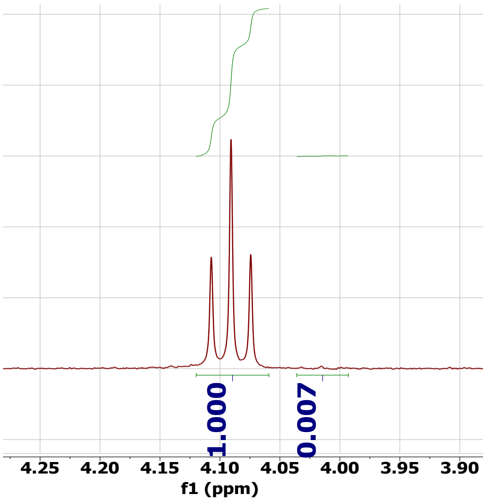

Figure S10. ^{1}H NMR spectroscopy of *Z*-AIZ 3 after addition of HCl, Related to "Accelerated *Z*- to *E*-reversion with weak acids". ^{1}H NMR spectroscopy of AIZ **3** after UV-induced *E*→*Z*-isomerization and addition of 2 equivalents of HCl, showing specifically the chemical shift of the $-CH_2-O-$aryl group of the *E*- (4.09 ppm) and *Z*-form (4.04 ppm). The negligible amount of *Z*-AIZ signifies the extent of catalytic destabilization of the *Z*-form by HCl.

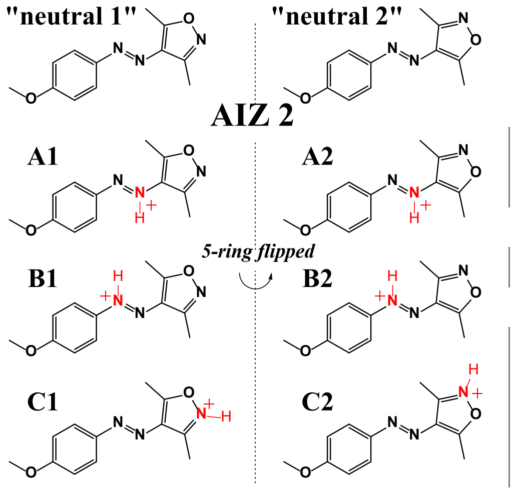

	E (EV)		
	E	*Z*	TS
neutral 1	0.11 (0.02)	0.57 (0.67)	1.88 (1.89)
Neutral 2	0.00 (0.00)	0.57 (0.68)	1.86 (1.89)
A1	0.11 (0.11)	0.39 (0.46)	1.25 (1.33)
A2	0.13 (0.13)	0.37 (0.43)	-
B1	0.07 (0.08)	0.45 (0.55)	1.32 (1.29)
B2	0.00 (0.00)	0.42 (0.52)	-
C1	0.35 (0.26)	0.83 (0.93)	-
C2	0.33 (0.24)	0.84 (0.94)	-

Figure S11. Relative Gibbs free energies of AIZH+ 2 by DFT (PCM/GD3BJ/B3LYP/6-31G*), Related to “Accelerated *Z*- to *E*-reversion with weak acids”. DFT computed relative energies (in eV) of various conformations in AIZ **2**. Corresponding data without empirical dispersion correction is given in parentheses.

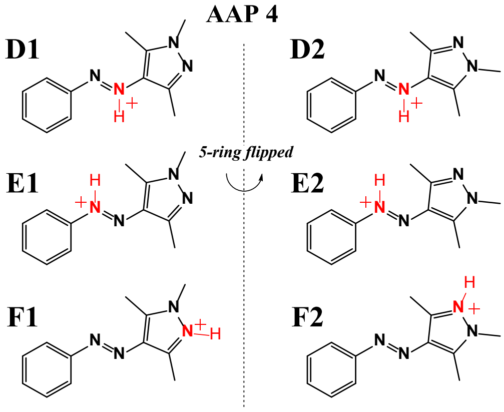

	E (EV)	
	E	*Z*
D1	0.48 (0.35)	0.76 (0.78)
D2	0.41 (0.33)	0.73 (0.77)
E1	0.18 (0.10)	0.51 (0.56)
E2	0.00 (0.00)	0.45 (0.49)
F1	0.23 (0.21)	0.73 (0.84)
F2	0.20 (0.16)	0.75 (0.82)

Figure S12. Relative Gibbs free energies of AAPH+ 4 by DFT (PCM/GD3BJ/B3LYP/6-31G*), Related to “Accelerated *Z*- to *E*-reversion with weak acids”. DFT computed relative energies of various conformations in AAP **4**. Protonation of the azo-nitrogen at the phenyl ring (structure E2/E1) is observed to be lowest in energy for both *E*- and *Z*-forms, consistent with results from Fuchter et al.[1] Corresponding data without empirical dispersion correction is given in parentheses.

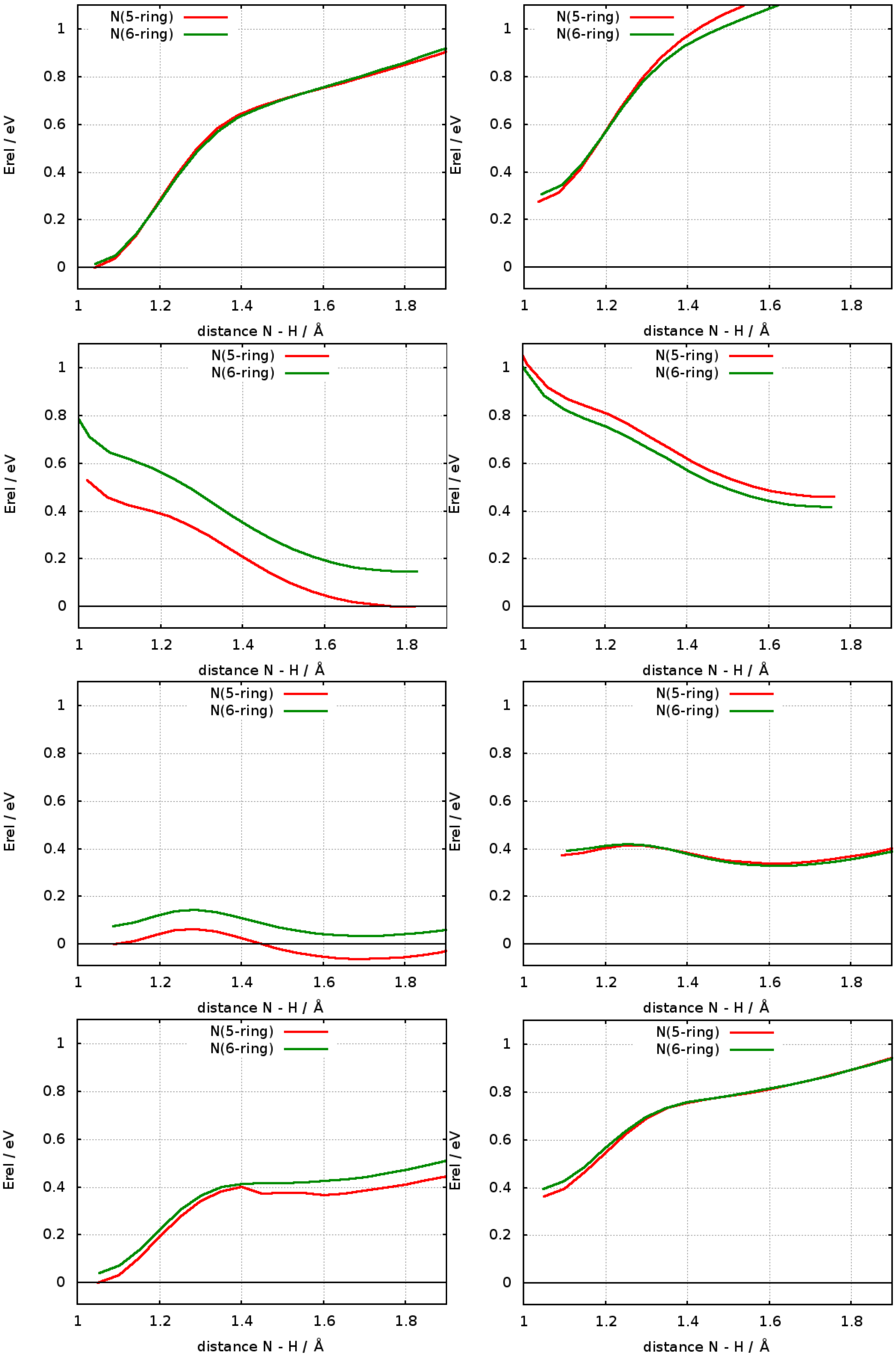

Figure S13. MEP scans for the deprotonation of AIZH+ 2 in presence of one adjacent molecule of acid (PCM/GD3BJ/B3LYP/6-31G*), Related to "Theoretical Analysis of the Z- to E- Thermal Conversion". Relative potential energies for the proton transfer between the CNNC unit of (left) *E*-AIZ **2** and (right) *Z*-AIZ **2** and one explicit molecule of (top) acetonitrile (solvent), (second row) acetic acid, (third row) trifluoroacetic acid, and (bottom) trifluoromethanesulfonic acid.

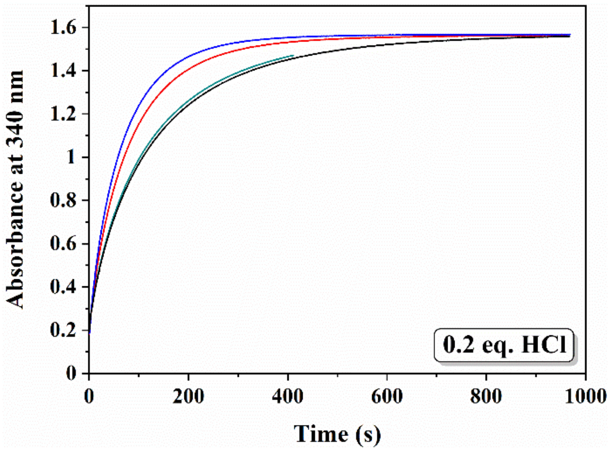

Figure S14. HCl-catalysed reversion of *Z*-AIZ 3 by UV/vis spectroscopy, Related to "Accelerated *Z*- to *E*-reversion with weak acids". Evolution in absorbance at 340 nm of AIZ **3** (70 μM in acetonitrile) after reaching the PSS_{365} (3 s) and adding 0.2 equivalents of HCl.

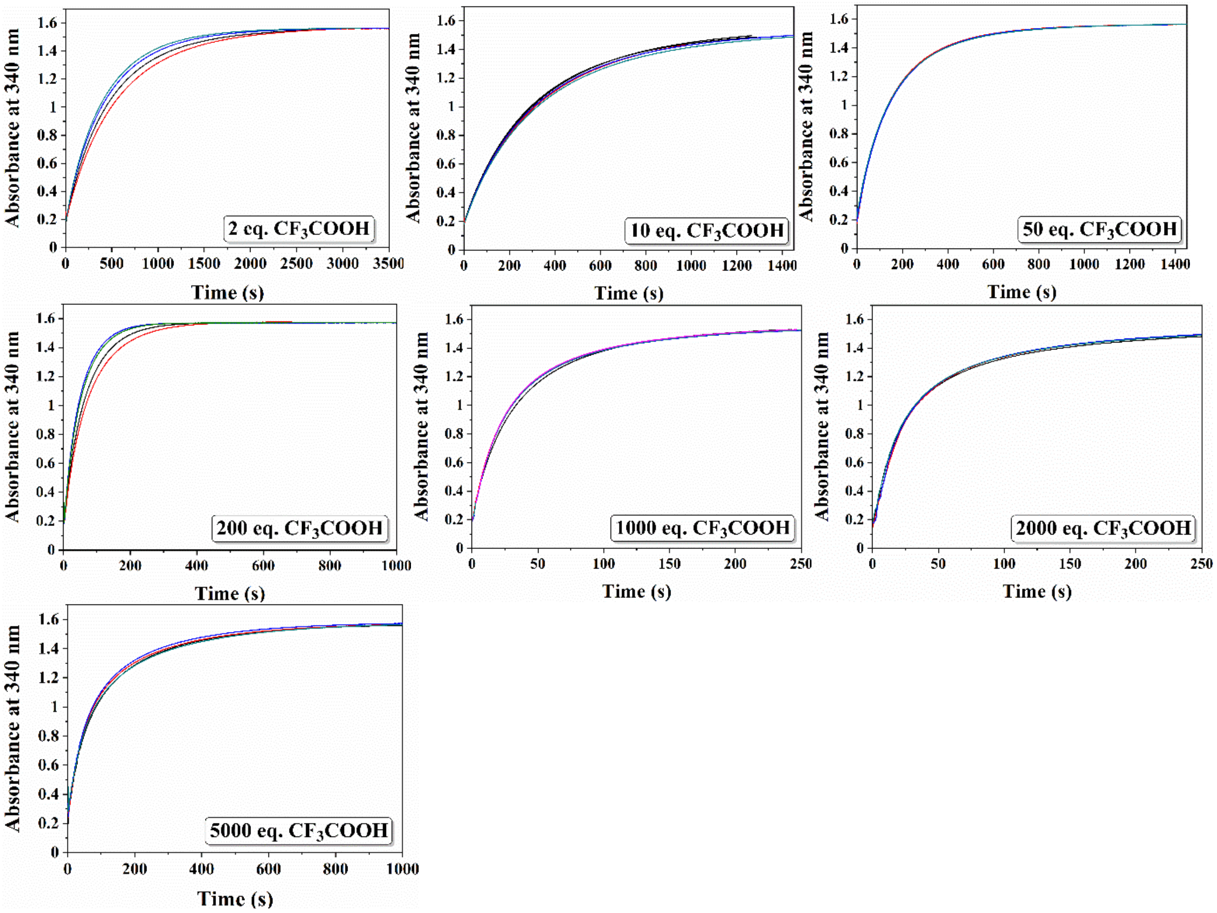

Figure S15. TFAA-catalysed reversion of *Z*-AIZ 3 by UV/vis spectroscopy, Related to "Accelerated *Z*- to *E*-reversion with weak acids". Evolution in absorbance at 340 nm of AIZ **3** (70 μM in acetonitrile) after reaching the PSS_{365} (3 s) and adding various equivalents of CF_3COOH. The half-lives and corresponding rate constants (k) are noted in Table 1.

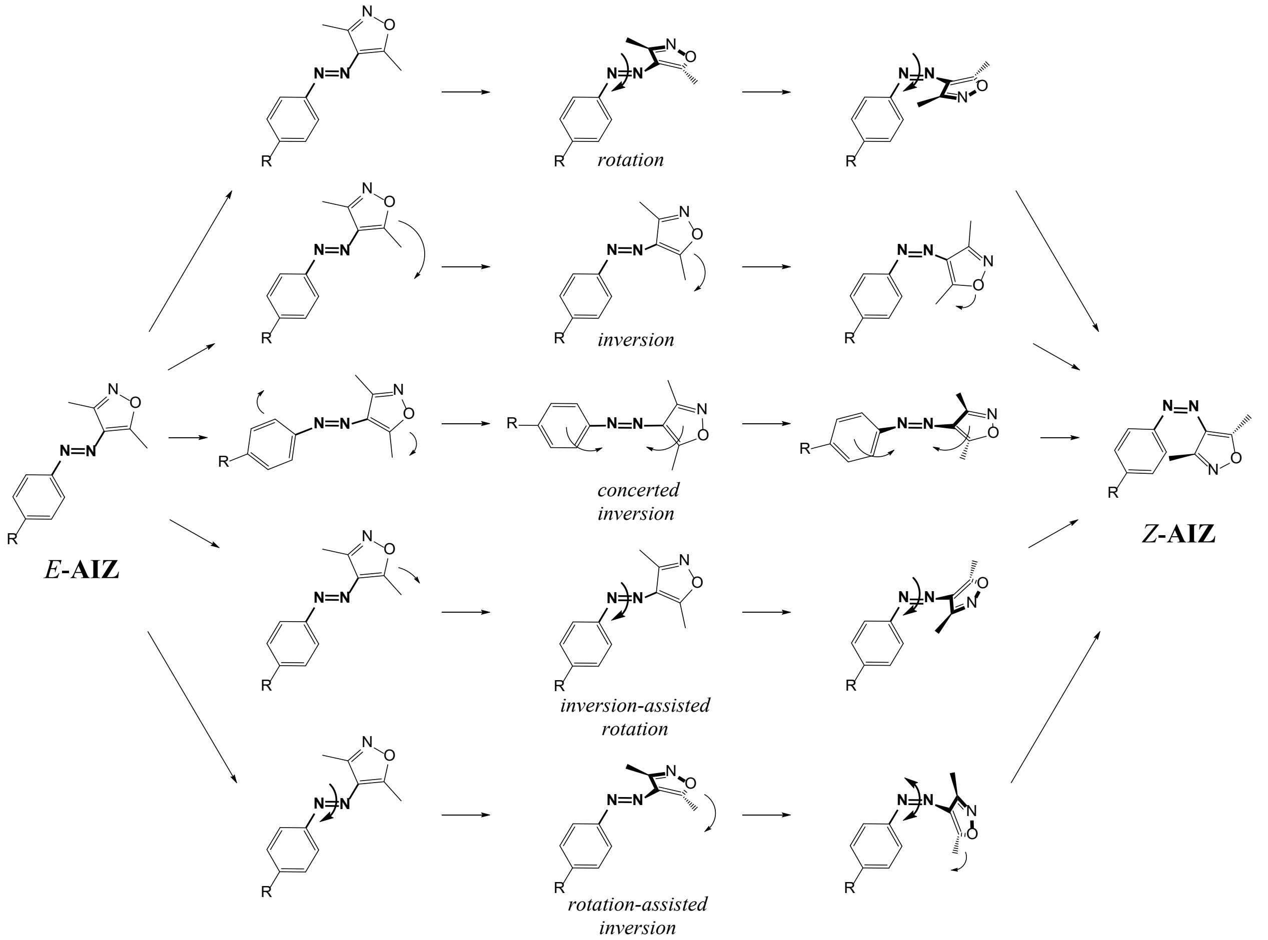

Scheme S1. Proposed mechanisms of Z- to E-AIZ reversion, Related to “Theoretical Analysis of the Z- to E- Thermal Conversion”. The thermal reversion pathways of azobenzenes have already been subject to many theoretical and experimental studies.[2,3,4,5,6] We propose the above AIZ isomerization pathways analogous to azobenzene-isomerization.

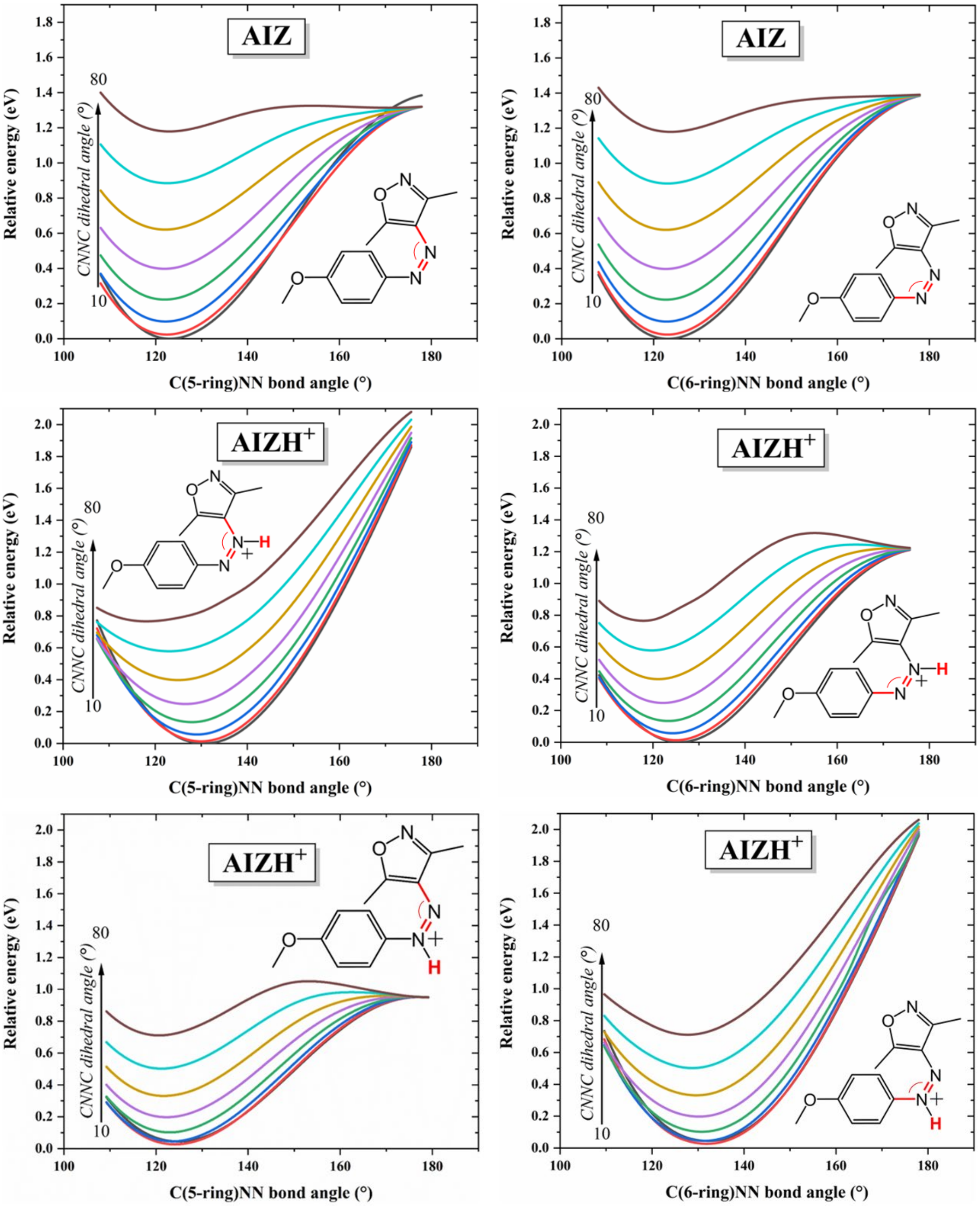

Figure S16. AIZ potential energy surfaces (PCM/GD3BJ/B3LYP/6-31G*), Related to "Theoretical Analysis of the Z- to E- Thermal Conversion". Relative potential energies along the coordinates dihedral angle CNNC (in increments of 10 degrees, starting from the *Z*-minimum) and either (left) C(5-ring)NN bond angle or (right) C(6-ring)NN bond angle of (top) AIZ **2** and (middle, bottom) AIZH$^+$ **2** (two positions of H$^+$).

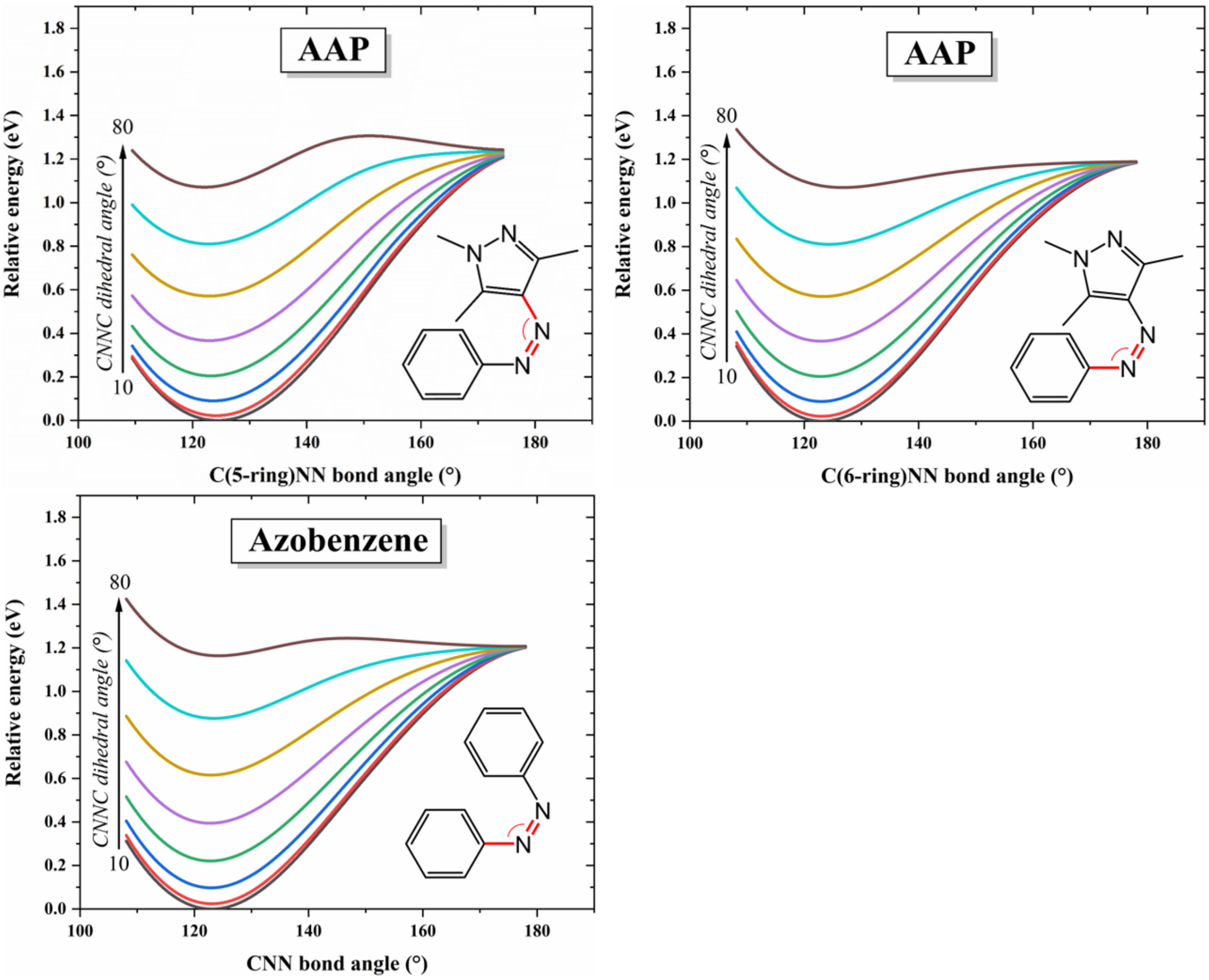

Figure S17. AAP and AB potential energy surfaces (GD3BJ/B3LYP/6-31G*), Related to "Theoretical Analysis of the *Z*- to *E*- Thermal Conversion". Relative potential energies of AAP **4** (top) along the coordinates dihedral angle CNNC (in increments of 10 degrees, starting from the *Z*-minimum) and either (top left) CNN (5-ring) bond angle or (top right) CNN (6-ring) bond angle. For the symmetric azobenzene (bottom) the CNN (6-ring) is the default.

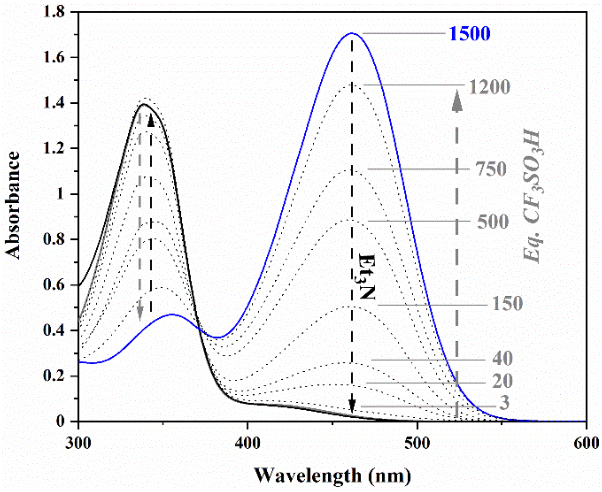

Figure S18. E-AIZH$^+$ by UV/vis spectroscopy, Related to "Thermally stable *Z*- and *E*-protonation with strong acids". UV/vis absorption spectrum of AIZ **3** (70 µM in acetonitrile) with increasing equivalents of CF_3SO_3H, reaching saturation at ca. 1500 eq (blue). Upon addition of excess Et_3N, the *E*-AIZ absorption is recovered with exception of a slight increase at 300 nm due to Et_3N (black).

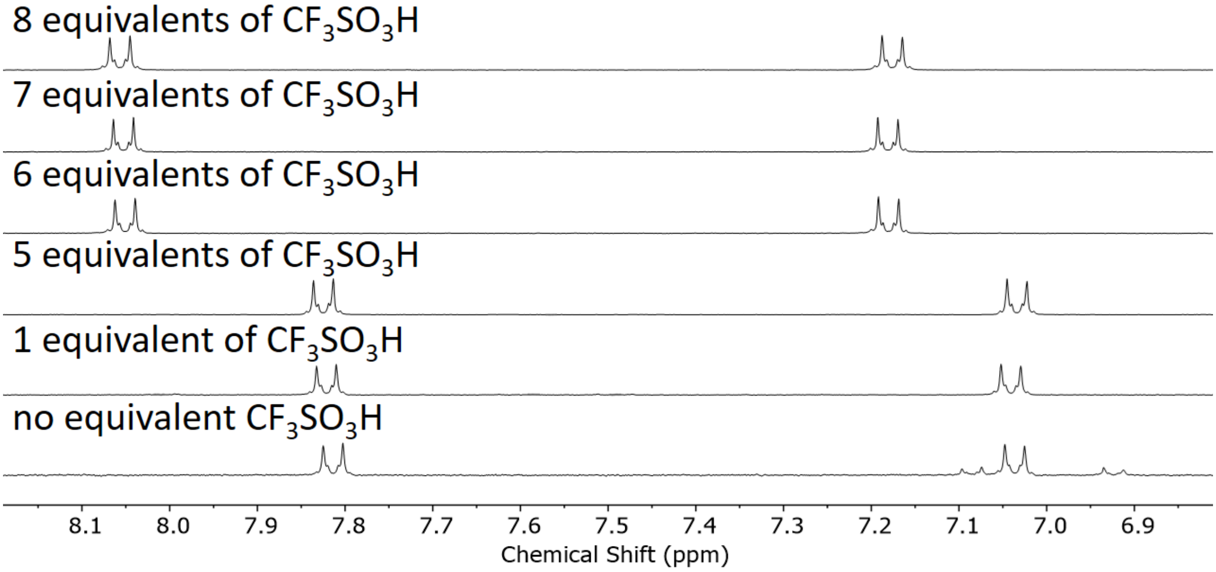

Figure S19. ^{1}H NMR spectroscopy of AIZH$^+$ 3 with CF_3SO_3H, Related to "Thermally stable *Z*- and *E*-protonation with strong acids". ^{1}H NMR spectroscopy of various samples of AIZ **3** (3.3 mM in CD_3CN) after addition of decreasing amounts of CF_3SO_3H. The striking difference between 5 and 6 equivalents of CF_3SO_3H is likely due to the low pH at such high concentrations versus results obtained in UV/vis absorbance spectroscopy at 70 µM concentration.

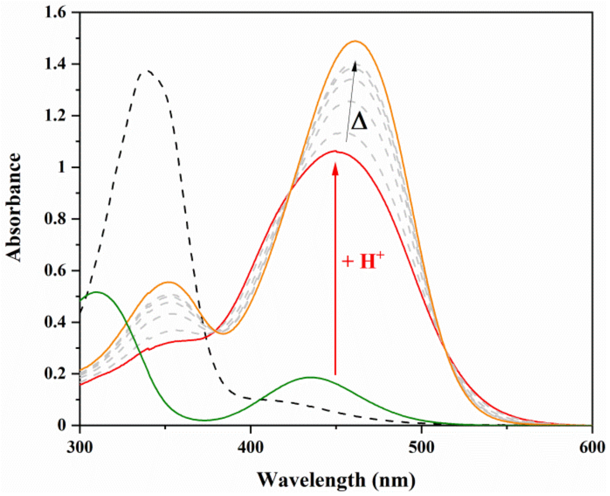

Figure S20. UV/vis spectroscopy of AIZH$^+$ 3 with CF_3SO_3H, Related to "Thermally stable *Z*- and *E*-protonation with strong acids". UV/vis absorption spectrum of AIZ **3** at the PSS$_{365nm}$ (70 µM in acetonitrile, black dashed line before and green solid line after irradiation), adding 1000 equivalents of CF_3SO_3H to form the *Z*-azonium species. Afterward, the *Z*-rich solution undergoes thermal conversion to the *E*-azonium species (grey dashed lines, 2 min intervals), with the orange line indicating thermal equilibrium at this concentration (orange spectrum taken after a total of 30 min).

Table S1. ^{1}H NMR chemical shifts of the unprotonated and protonated isomers of AIZ 3, Related to “Thermally stable *Z*- and *E*-protonation with strong acids”. Comparison of chemical shifts (in ppm) of the protonated and unprotonated *E*- and *Z*-forms of AIZ **3** (ca. 3 mM in CD$_3$CN, with 45 mM of CF$_3$SO$_3$H for the protonated species, *E*-*Z* isomerization prior to adding acid by irradiation at 365 nm).

	Ar-H	Ar-H	O-CH$_2$	-CH$_3$	-CH$_3$	-CH$_2$-	-(CH$_2$)$_2$-	-CH$_3$
E-AIZ 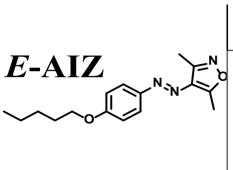	7.81 (*d*) J = 8.97 Hz	7.03 (*d*) J = 8.98 Hz	4.06 (*t*) J = 6.58 Hz	2.70 (*s*)	2.47 (*s*)	1.81-1.76 (*m*)	1.48-1.37 (*m*)	0.94 (*t*) J = 6.95 Hz
Z-AIZ 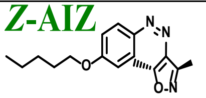	7.09 (*d*) J = 9.00 Hz	6.92 (*d*) J = 9.09 Hz	3.99 (*t*) J = 6.57 Hz	2.09 (*s*)	1.75 (*s*)	1.74-1.69 (*m*)	1.45-1.35 (*m*)	0.92 (*t*) J = 6.95 Hz
E-AIZH$^+$ 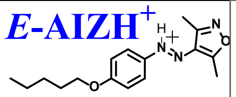	8.01 (*d*) J = 9.16 Hz	7.15 (*d*) J = 9.17 Hz	4.15 (*t*) J = 6.58 Hz	2.82 (*s*)	2.64 (*s*)	1.85-1.78 (*m*)	1.48-1.35 (*m*)	0.94 (*t*) J = 7.08 Hz
Z-AIZH$^+$ 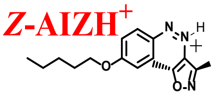	7.86 (*d*) J = 9.12 Hz	7.17 (*d*) J = 9.26 Hz	4.22 (*t*) J = 6.60 Hz	2.59 (*s*)	1.86 (*s*)	1.85-1.78 (*m*)	1.48-1.35 (*m*)	0.93 (*t*) J = 7.06 Hz

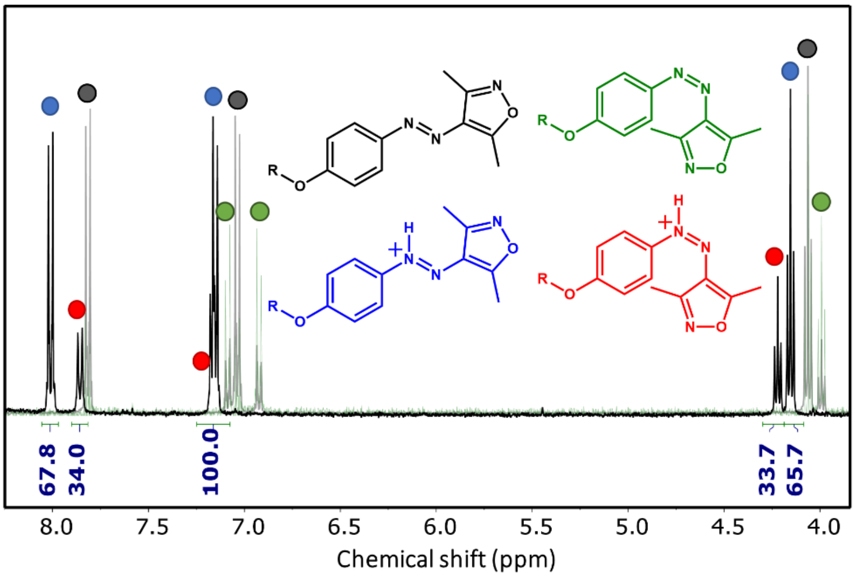

Figure S21. Comparison of chemical shifts of all AIZ 3 species in ^{1}H NMR spectroscopy, Related to “Thermally stable *Z*- and *E*-protonation with strong acids”. ^{1}H NMR spectroscopy of AIZ 3 in CD$_3$CN in its different unprotonated and protonated forms. *E*-AIZ (black) can be observed immediately, and addition of 15 eq. of CF$_3$SO$_3$H provides *E*-AIZH$^+$ (blue). *Z*-AIZ (green) is generated by irradiation at 365 nm (radiant flux 1.2 W), with *Z*-AIZH$^+$ (red) formed after addition of 15 eq. of CF$_3$SO$_3$H hereto.

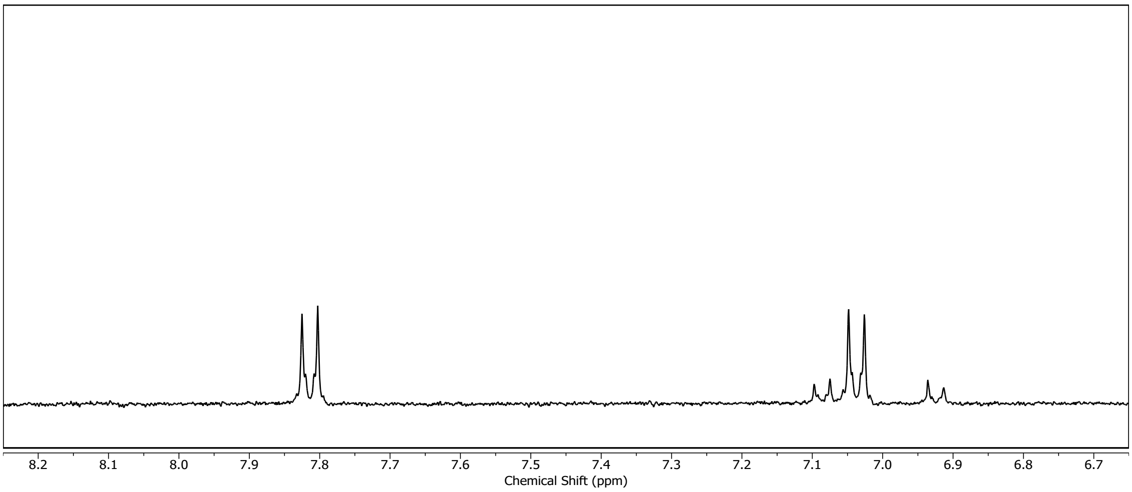

Figure S22. ^{1}H NMR spectroscopy of AIZ 3 upon addition of CF_3SO_3Li, Related to "Thermally stable *Z*- and *E*-protonation with strong acids". ^{1}H NMR spectroscopy of AIZ **3** (3.3 mM in CD_3CN) after addition of 15 eq. of CF_3SO_3Li (i.e., 49.5 mM, equal to the amount of CF_3SO_3H added in Figure 4). The chemical shifts of the unprotonated *E*- and *Z*-isomers are observed, whereas even low equivalents of CF_3SO_3H destabilize the *Z*-AIZ form, suggesting an insignificant influence of ionic strength on chemical speciation.

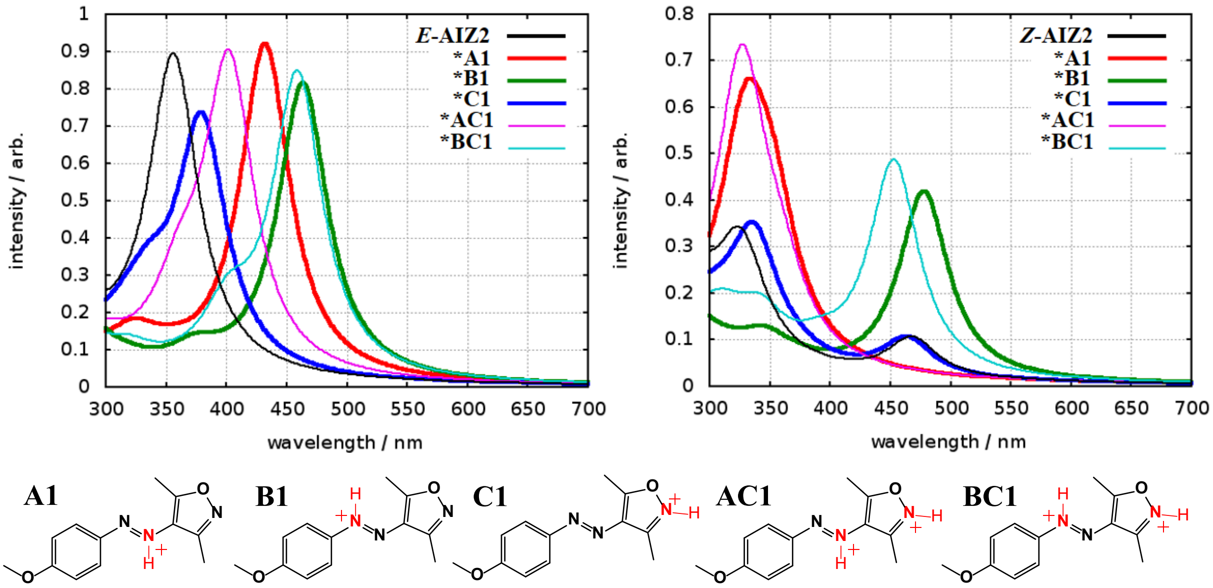

Figure S23. Calculated absorption spectra of singly and doubly protonated AIZ 2's, Related to "Azonium formation in azoheterocycles". Computed UV/vis absorbance spectra of the indicated singly and doubly protonated AIZ **2** species in the (left) *E*- and (right) *Z*-configuration. The corresponding spectrum for the neutral species is additionally shown as reference (black).

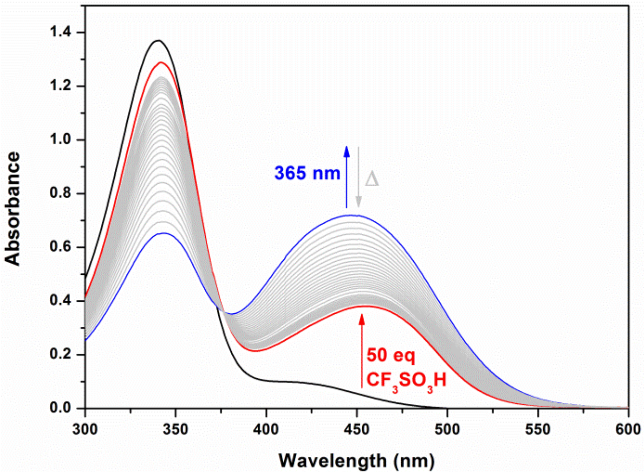

Figure S24. Thermal reversion to E-AIZH$^+$ with CF_3SO_3H by UV/vis spectroscopy, Related to "Thermally stable *Z*- and *E*-protonation with strong acids". UV/vis absorption spectrum of AIZ **2** (70 µM in acetonitrile, black line) after addition of 50 eq CF_3SO_3H (red line) and with subsequent irradiation at 365 nm (blue line). The *E*-form thermally relaxes back to *Z* over time (grey lines, 1 min intervals).

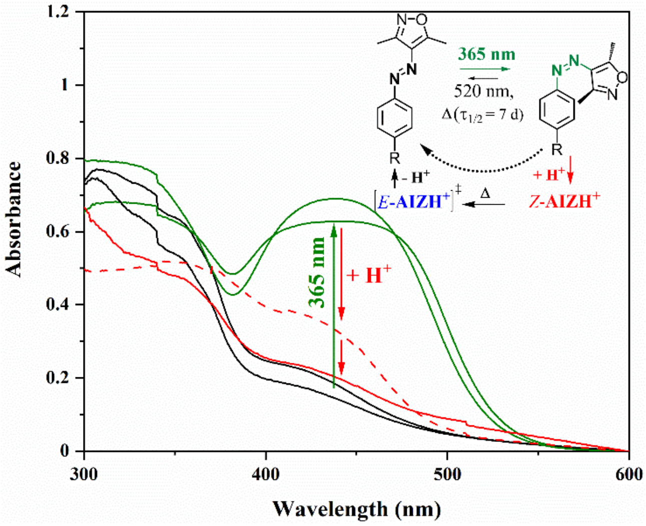

Figure S25. AIZ 3 thin layer solid state switching by UV/vis spectroscopy, Related to "Acid-Catalysed Liquid-to-Solid Phase Transitioning". UV/vis absorption spectra of a thin film of **3** pressed between 2 glass slides before (black solid) and after (green solid) irradiation at 365 nm with concurrent solid-to-liquid phase-transitioning. The *Z*- to *E*-reversion proceeds through irradiation at 520 nm as shown previously (back to black solid). Upon introduction of CF_3COOH vapours to the liquefied thin film (reliquefied by 365 nm irradiation, following the green arrow) acid-catalysed *Z* → *E*-reversion occurs (following the red arrow to the red dashed and subsequently red solid line, 1 min intervals).

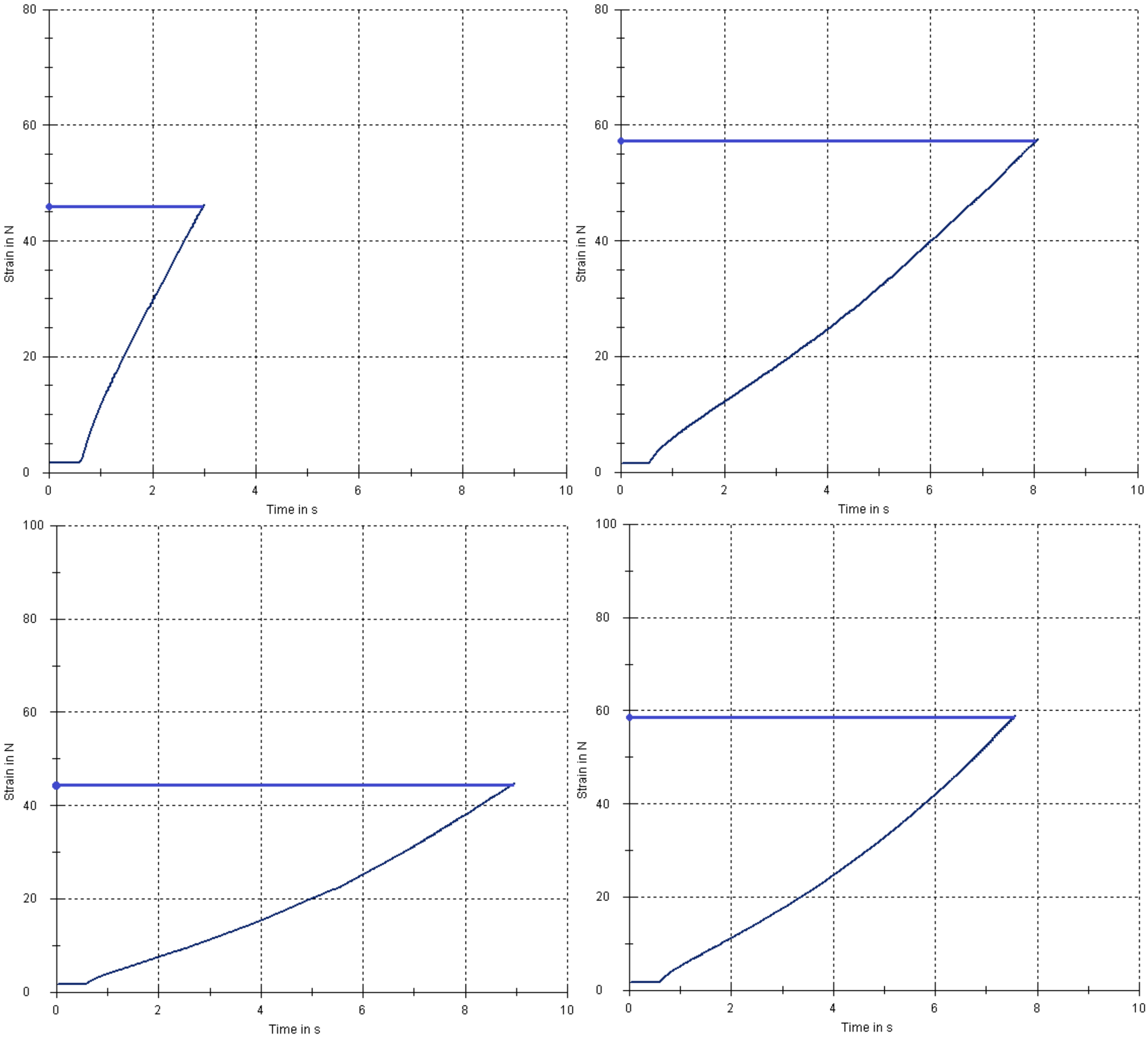

Figure S26. Tensometry of AlZ 3 at aluminium slides, Related to "Acid-Catalysed Adhesion". Tensile strength measurements of 4 pairs of aluminium slides conjoined at a 1.0 by 1.4 cm area with 3.4 mg of **3** as shown in Scheme 5, showing break points at 36.6 ± 5.2 N cm^{-2}.

SUPPORTING EXPERIMENTAL PROCEDURES

All starting materials were purchased from Sigma-Aldrich (Sigma-Aldrich Corp., St. Louis, Missouri, USA) and Alfa Aesar (Alfa Aesar, Ward Hill, Massachusetts, USA), and used without further purification.

UV/vis absorption spectra were recorded with a Jasco V750 double-beam spectrophotometer and processed with F. Menges' Spectragryph - optical spectroscopy software, v1.2.11. Irradiation of the samples in solution (acetonitrile) and in the solid state was carried out with light-emitting diodes at 365 nm (UV LED Gen2 Emitter, LED Engin Inc., San Jose, California, USA, radiant flux 1.2 W) and 520 nm (LSC-G HighPower-LED, Cree Inc., Durham, North Carolina, USA, radiant flux 87 lm). The NMR spectra for the characterization were recorded on an AV-300-spectrometer with 300.1 Hz (1H) and 75.5 Hz (13C) (Bruker, Billerica, Massachusetts, USA). For monitoring the photostationary states, a DD2-600-spectrometer with 600 Hz (1H) and 151 Hz (13C) was employed (Agilent Technologies, Santa Clara, California, USA). Chemical shifts (δ) are reported in parts per million with respect to tetramethylsilane, referenced to residual solvent (CD2HCN, CD2ClH or DMSO-d5) signals, and coupling constants are denoted in hertz. Integrations are reported, with multiplicities denoted as: s = singlet, d = doublet, t = triplet, br = broad singlet, m = multiplet. MestReNova 12.0.4 (Mestrelab Research S.L., Santiago de Compostela, Spain) was used to analyse all NMR spectra. Mass spectra were recorded on a MicroTof ESI (Bruker Daltonics, Bremen, Germany) through Electrospray ionization (ESI) from methanol. Optical microscopy was performed with an Olympus CKX 41 microscope operated with an Olympus XC 10 camera, and their processing was done with the software Stream Essentials v1.9. Tensile measurements were conducted on a Zwicki 1120 ZW2.5/TH1S tensile test machine.

Solidification through acid vapours

In all cases described in the paper, ca. 100 µL of the involved acid was transferred to a 2 mL vial. A Pasteur pipette was used to transfer the acid vapours from the headspace after several pumps to equilibrate the headspace and pipette. With a volume uptake of about a millilitre, the pipette end is transferred to ca. 5 mm above the surface with Z-AIZ, followed by a gradual release over ca. 2 seconds while moving to cover the whole surface.

Adhesion experiments

Glass microscope slides (76 mm x 26 mm) from Servoprax GmbH, Wesel, Germany, were cut into 1.4 x 2.6 cm slides and washed with water and acetone. A scratch 1.0 cm into the slide marked the 1.4 cm2 area on which 2.2 mg of AIZ was weighed out. Following a UV-induced solid-to-liquid phase transition, fumes of 99.99% CF3COOH were blown over the liquid phase Z-AIZ with a glass pipette as described above. Directly after emptying the content fumes over the sample the slides were quickly pressed together, to be left for 2 hours clamped between a household clothespin to ensure maximum coverage of the acid-catalysis. Afterwards, weights were hung incrementally from custom-made slide holders (see Figure 5) until reaching the breaking point. In the case of probing the thermal adhesion with acid fumes present, fumes of 99.99% CF_3COOH were blown over molten *E*-AIZ **3** while keeping the corresponding glass slides at a temperature of 80 °C on a hot plate, followed by swiftly conjoining the slides. The plexiglass and aluminium slides were custom cut to shape by the University workshop, further experimental steps were performed identically to the glass adhesion method described here.

Syntheses

AIZs **2** (MP: 106 °C) and **3** (MP: 66 °C) were available from a previous study,[7] AIZ **1** (MP: 54 °C) was synthesized using the same synthetic method. The procedure for AAP **4** (MP: 57 °C) was reported previously,[8] and could be synthesized from the pentadione intermediate also.

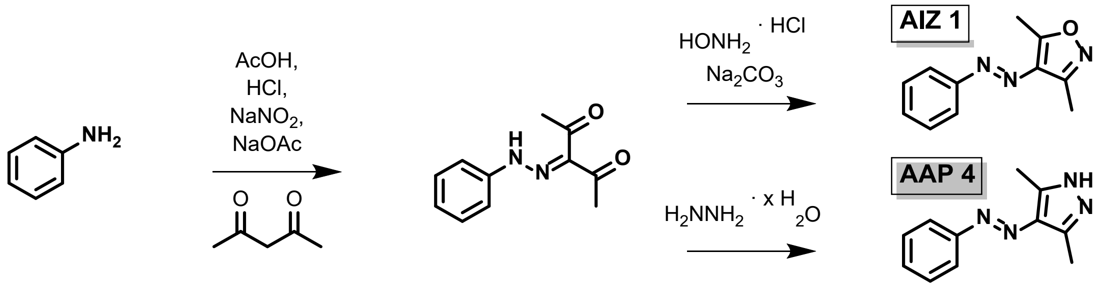

Scheme S2. Synthetic procedure to AIZ 1 and AAP 4.

General Procedure I: Synthesis of alkoxy 3-(2-phenylhydrazono)pentane-2,4-diones

A solution of the aniline (1.0 eq.) in AcOH (1.5 mL/mmol) and HCl (12 M, 0.23 mL/mmol) was cooled to 0 °C and $NaNO_2$ (1.2 eq.) in a small amount of H_2O was added dropwise. This mixture was stirred for 45 min at 0 °C. Afterwards the diazonium salt was added to a suspension of pentane-2,4-dione (1.3 eq.) and NaOAc (3.0 eq.) in a mixture of EtOH (1.0 mL/mmol) and H_2O (0.60 mL/mmol) and stirred overnight. The precipitate was filtered and washed several times with H_2O to yield the desired compound.

3-(2-phenylhydrazineylidene)pentane-2,4-dione (X)

Yield: 1.08 g (5.29 mmol, 98%).

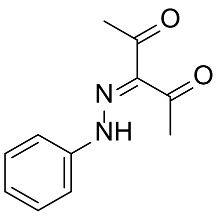

^{1}H-NMR: (300 MHz, $CDCl_3$) δ = 14.74 (s, 1H), 7.50–7.33 (m, 4H), 7.24–7.16 (m, 1H), 2.61 (s, 3H), 2.49 (s, 3H) ppm.

^{13}C-NMR: (75 MHz, $CDCl_3$) δ = 198.0, 197.2, 141.6, 133.3, 129.7, 126.0, 116.3, 31.8, 26.7 ppm.

MS (*m/z*): (ESI, MeOH) Calc. for $[C_{11}H_{12}N_2O_2Na]^+$: 227.0796; found 227.0797.

General Procedure II - AIZs

To a suspension of pentanedione (1.0 eq.) in EtOH (10 mL/mmol) were added Na_2CO_3 (1.5 eq.) and hydroxylamine hydrochloride (1.5 eq.) and this mixture was stirred at 80 °C for 18 h. The solvent was removed under reduced pressure and the crude product was purified by column chromatography (silica, CH/EtOAc 20:1). After recrystallisation in EtOH the target molecule was washed with ice-cold EtOH (3×) and lyophilized to obtain a yellow solid.

(E)-3,5-dimethyl-4-(phenyldiazenyl)isoxazole (AIZ 1)

Yield: 153 mg (0.760 mmol, 78%).

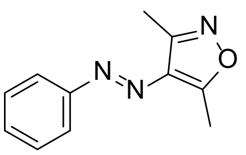

^{1}H-NMR: (300 MHz, $CDCl_3$) δ = 7.86–7.76 (m, 2H), 7.56–7.34 (m, 3H), 2.76 (s, 3H), 2.54 (s, 3H) ppm.

^{13}C-NMR: (75 MHz, $CDCl_3$) δ = 169.6, 153.9, 153.0, 130.9, 129.6, 129.2, 122.3, 12.3, 11.8 ppm.

MS (*m/z*): (ESI, MeOH) Calculated for $[C_{11}H_{11}N_3OH]^+$: 202.09749; found 202.09736.

MP: 54 °C

General Procedure II - AAPs

Methylhydrazine or hydrazine x hydrate (1eq.) was added to a solution of desired 3-(2-phenylhydrazono)pentane-2,4-dione (1eq.) dissolved in EtOH and refluxed for 3 hours. Concentration under reduced pressure yielded the resulting arylazopyrazole without further purification.

(E)-1,3,5-trimethyl-4-(phenyldiazenyl)-1H-pyrazole (AAP 4)

Yield: 196 mg (0.915 mmol, 94%).

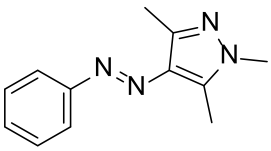

^{1}H-NMR: (400 MHz, $CDCl_3$) δ = 7.82–7.74 (m, 2H), 7.50–7.42 (m, 2H), 7.41–7.32 (m, 1H), 3.78 (s, 3H), 2.58 (s, 3H), 2.50 (s, 3H) ppm.

^{13}C-NMR: (101 MHz, $CDCl_3$) δ = 153.8, 142.6, 138.9, 135.3, 129.4, 129.0, 121.9, 36.1, 14.0, 10.1 ppm.

MS (*m/z*): (ESI, MeOH) Calculated for $[C_{12}H_{14}N_4Na]^+$: 237.11107; found 237.11108.

MP: 57 °C

DFT Calculations

All DFT calculations were performed with the Gaussian 09 Rev. D.01 package[9] employing the B3LYP hybrid functional[10] and the 6-31G* basis set.[11] The standard convergence criteria for geometry optimizations and single point calculations were used, along with the addition of empirical dispersion correction of type Grimme D3 with Becke-Johnson damping.[12,13,14] No counterions were employed for the cationic species. To include solvent effects of Acetonitrile into the calculations, the polarizable continuum model (PCM)[15,16,17] was used and the cavity for the molecule was formed based on the UFF model for atomic radii.[18] UV/vis spectra were obtained for the ground state optimized structures from TDDFT calculations of the lowest 100 excited states employing a Lorentzian line broadening of 50 nm (fwhm). For the visualization of molecular geometries VMD 1.9.3 with the internal Tachyon renderer was used.[19,20] Minimum energy profiles for the ground state along the dihedral angle coordinate CNNC in the interval [70,110] degrees were calculated starting from the E and Z optimized structures, respectively, followed by a harmonic fit to yield the transition state energy. Gibbs free energies were obtained accordingly by including zero point and thermodynamic corrections resulting from additional harmonic frequency calculations for standard temperature T= 298.15 K. Reaction rate constants and half-life times were subsequently calculated using the standard relations:

$$k(T) = \frac{k_B T}{h} \mathrm{e}^{-\frac{\Delta G^{\ddagger}}{RT}}$$

$$\tau_{1/2} = \ln(2)\tau = \ln(2)\frac{1}{k}.$$

In order to address the proton transfer within the azo-moiety, minimum energy profiles for the transfer to/from one explicit molecule of MeCN, CH_3COOH, CF_3COOH, and CF_3SO_3H were performed, starting out of the corresponding minimized geometry.

SUPPORTING REFERENCES

---

[1] R. S. L. Gibson, J. Calbo, and M. J. Fuchter, *ChemPhotoChem*, **2019**, 3, 372–377.

[2] H. M. D. Bandara, and S. C. Burdette, *Chem. Soc. Rev.*, **2012**, 41, 1809–1825.

[3] J. Fregoni, G. Granucci, M. Persico, and S. Corni, *Chem*, **2020**, 6, 250–265.

[4] J. Dokić, M. Gothe, J. Wirth, M. V. Peters, J. Schwarz, S. Hecht, and P. Saalfrank, *J. Phys. Chem. A*, **2009**, 113, 6763–6773.

[5] L. Zhou, L. Chen, G. Ren, Z. Zhu, H. Zhao, H. Wang, W. Zhang, and J. Han, *Phys. Chem. Chem. Phys.*, **2018**, 20, 27205–27213.

[6] D. L. Isac, A. Airinei, M. Homocianu, N. Fifere, C. Cojocaru, and C. Hulubei, *J. Photochem. Photobiol. A Chem.*, **2020**, *390*, 112300.

[7] L. Kortekaas, J. Simke, D. W. Kurka, and B. J. Ravoo, *ACS Appl. Mater. Interfaces,* **2020**, *12*, 32054–32060.

[8] L. Stricker, E.-C. Fritz, M. Peterlechner, N. L. Doltsinis, and B. J. Ravoo, *J. Am. Chem. Soc.*, **2016**, *138*, 4547–4554.

[9] J. Frisch, G. W. Trucks, H. B. Schlegel, G. E. Scuseria, M. A. Robb, J. R. Cheeseman, G. Scalmani, V. Barone, B. Mennucci, G. A. Petersson, H. Nakatsuji, M. Caricato, X. Li, H. P. Hratchian, A. F. Izmaylov, J. Bloino, G. Zheng, J. L. Sonnenberg, M. Hada, M. Ehara, K. Toyota, R. Fukuda, J. Hasegawa, M. Ishida, T. Nakajima, Y. Honda, O. Kitao, H. Nakai, T. Vreven, J. A. Montgomery, Jr., J. E. Peralta, F. Ogliaro, M. Bearpark, J. J. Heyd, E. Brothers, K. N. Kudin, V. N. Staroverov, R. Kobayashi, J. Normand, K. Raghavachari, A. Rendell, J. C. Burant, S. S. Iyengar, J. Tomasi, M. Cossi, N. Rega, J. M. Millam, M. Klene, J. E. Knox, J. B. Cross, V. Bakken, C. Adamo, J. Jaramillo, R. Gomperts, R. E. Stratmann, O. Yazyev, A. J. Austin, R. Cammi, C. Pomelli, J. W. Ochterski, R. L. Martin, K. Morokuma, V. G. Zakrzewski, G. A. Voth, P. Salvador, J. J. Dannenberg, S. Dapprich, A. D. Daniels, O Farkas, J. B. Foresman, J. V. Ortiz, J. Cioslowski, and D. J. Fox, “Gaussian 09 Revision D.01”, Gaussian Inc. Wallingford CT (**2013**).

[10] P. J. Stephens, F. J. Devlin, M. J. Frisch, C. F. Chabalowski, *J. Phys. Chem.* **1994**, *98*, 11623-27.

[11] M. M. Francl, W. J. Pietro, W. J. Hehre, J. S. Binkley, D. J. DeFrees, J. A. Pople, and M. S. Gordon, *J. Chem. Phys.* **1982**, *77*, 3654-65.

[12] S. Grimme, J. Antony, S. Ehrlich, and H. Krieg, J. Chem. Phys., 2010, 132, 154104.

[13] S. Grimme, S. Ehrlich, and L. Goerigk, J. Comput. Chem, 2011, 32, 1456.

[14] D. G. Smith, L. A. Burns, K. Patkowski, and C. D. Sherrill, J. Phys. Chem. Lett., 2016, 7, 2197.

[15] S. Miertuš, E. Scrocco, J. Tomasi, *Chemical Physics* **1981**, *55*, 117–129.

[16] R. Improta, V. Barone, G. Scalmani, M. J. Frisch, *J. Chem. Phys.* **2006**, *125*, 054103.

[17] R. Improta, G. Scalmani, M. J. Frisch, V. Barone, *J. Chem. Phys.* **2007**, *127*, 074504.

[18] A. K. Rappé, C. J. Casewit, K. S. Colwell, W. A. Goddard III, W. M. Skiff, *J. Am. Chem. Soc.* **1992,** *114*, 10024-10035.

[19] W. Humphrey, A. Dalke, K. Schulten, **1996**, *14*, 33–38.

[20] J. Stone, “*An Efficient Library for Parallel Ray Tracing and Animation”*, Master’s thesis, Computer Science Department, University of Missouri-Rolla (**1998**).